ACS OMEGA

Open Access

http://pubs.acs.org/journal/acsodf

Article

Understanding Cholesterol−Mycolic Acid−Phosphatidylcholine Interactions: Advancing Electrochemical Detection of Tuberculosis

Nsovo S. Mathebula, Okoroike C. Ozoemena, Patrick V. Mwonga, Aderemi B. Haruna, and Kenneth I. Ozoemena*

Cite This: *ACS Omega* 2025, 10, 50813−50824

Read Online

ACCESS | Metrics & More | Article Recommendations | Supporting Information

ABSTRACT: Immunodetection of active tuberculosis (TB), including in human immnodeficiency virus (HIV)-positive patients, is crucial for effective treatment and disease elimination. Mycolic acid (MA) is a key antigen for detecting TB antibodies, although antimycolic acid antibodies (AMAAs) have not yet been isolated. However, AMAA levels are elevated in TB-infected patients and can interact with mycolic acid antigen (MAA). A significant challenge in TB detection arises from the cross-reactivity of cholesterol (Ch) and anticholesterol antibodies (AChAs) due to the cholesteroid nature of MAA. For the first time, the cholesteroidal nature of MAA has been established through electrochemical experiments and supported by theoretical density functional theory (DFT) calculations. An electrochemical TB immunosensor was developed by using a glassy carbon electrode modified with MAA-confined activated carbon (GCE−AC−MAA). Electrochemical analysis of TB-positive serum revealed activity similar to that of AChA in the presence of phosphatidylcholine (PC)/MAA, demonstrating cross-reactivity. The optimal detection protocol involved preincubating TB serum in liposomes to free AMAA, followed by electrochemical immunosensor detection. DFT calculations showed that cholesterol interacts with MAA (p-band center, ε_p = −11.3922 eV) but more strongly in the presence of PC/MAA (ε_p = −11.2695 eV). As the p-band center approaches the Fermi level, the bond length between cholesterol and the adsorbent shortens, increasing the interaction strength. The results indicate that the shorter the bond length between the adsorbate (Ch) and the adsorbent (PC, MA, or PC/MA), the stronger the p-band center (i.e., strong binding to the atomic nucleus). These findings provide valuable insights for improving TB immunodetection strategies.

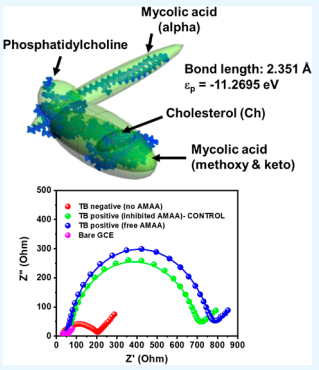

INTRODUCTION

Tuberculosis (TB), caused by the bacterium *Mycobacterium tuberculosis*, is one of the top 10 causes of death worldwide.[1] The disease spreads when individuals with active TB expel bacteria into the air through coughing. Despite being discovered over a century ago, TB remains a global epidemic and a major public health issue, affecting approximately a quarter of the global population.[2] However, most people infected with *M. tuberculosis* will not develop active TB disease, and some may clear the infection.[3,4] As of 2021, an estimated 10.6 million people have developed TB, with 6 million being men, 3.4 million women, and 1.6 million children. Additionally, the World Health Organization (WHO) reported that approximately 1.6 million people died from TB in 2021, making it the leading cause of death from a single infectious agent.[1,5] Over 95% of TB deaths occur in low- and middle-income countries, and the disease is among the top three causes of mortality for women aged 15−44 years.[6]

Mycobacterium tuberculosis (MTB) is an aerobic, Gram-positive, nonspore-forming, nonmotile, and slow-growing bacillus with a curved, beaded, rod-shaped morphology. Its remarkable hardiness enables it to survive under adverse environmental conditions.[7] The cell wall of MTB is extremely hydrophobic and forms a robust permeability barrier, making it naturally resistant to a wide range of antimicrobial agents.[7,8] Additionally, the cell wall's complex structure, resulting from its unique chemical composition, sets it apart from other bacteria,[9] making it one of the most intricate bacterial membranes. This complexity contributes to the bacterium's resistance to numerous drugs.[10]

The MTB cell wall consists of an inner layer and an outer layer.[11,12] The outer layer is composed of lipids and proteins, while the inner layer includes peptidoglycan, arabinogalactan, and mycolic acid. The peptidoglycan is linked to arabinogalactan (D-arabinose and D-galactose), which is covalently bonded to high-molecular-weight mycolic acids.[13]

Mycolic acid antigens (MAAs) are very long-chain (C60−C90) alpha-alkyl-beta-hydroxy fatty acids that account for approximately 30% of the dry weight of *Mycobacterium tuberculosis* (MTB).[14,15] These antigens are the major lipid component of the MTB envelope, playing a crucial role in

Received: February 3, 2025
Revised: August 20, 2025
Accepted: September 24, 2025
Published: October 22, 2025

resistance to both drugs and oxidative stress.[16,17] Mycolic acids consist of two distinct parts: a long fatty meromycolate chain and a saturated carboxylic mycolic motif. The meromycolate chain varies in pathogenic mycobacteria based on the type and spacing of functional groups, leading to the classification of mycolic acids into three structural subclasses: alpha-, methoxy-, and keto-mycolates.[18] Alpha-mycolates contain no oxygen functional groups in their meromycolate chain, whereas methoxy- and keto-mycolates have either a methoxy or keto group, along with methyl branches near the oxygenated groups.[18,19] It has been well established that the oxygenated mycolates exhibit more antigenicity than the alpha-mycolates with respect to antimycolic acid antibody (AMAA) recognition and that cross-reactive antibodies binding to both MA and cholesterol exist in human sera. Keto-mycolates favor a rigid, fully folded W-shaped conformation, while alpha- and methoxy-mycolates exhibit partially folded structures.[20−22] Mycolic acid (MA) is a key antigen for detecting TB antibodies, although antimycolic acid antibodies (AMAAs) have not yet been isolated, thus it is not commercially available, which makes it impossible to quantitatively determine its concentration in human serum.[11,12,23−25]

Numerous studies have identified mycolic acids as promising mycobacterial antigens for the serodiagnosis of active TB. They have been successfully utilized in various diagnostic methods, including enzyme-linked immunosorbent assay (ELISA),[11] optical biosensors,[12] electrochemical impedance spectroscopy (EIS),[23] and EIS-based mycolic acid antibody real-time inhibition techniques.[24,25] However, it was reported more than two decades ago by Schleicher et al. (2002)[11] that the use of free MAA for serodiagnosis of TB led to poor accuracy of only 57%. This poor accuracy was hypothesized to be due to molecular mimicry where the free MAA could fold and resemble a "cholesteroid" shape. Thus, it is highly possible that the cholesteroidal nature of MAA could lead to cross-reactivity of cholesterol and anticholesterol antibodies (AChAs). In 2008, Benadie et al. investigated this hypothesis using a resonant mirror biosensor and claimed to be the case.[26] Ranchod et al., in 2018, used recombinant chicken antibodies to investigate the antigenicity and cholesteroid nature of mycolic acids and further confirmed the dominant antigenic nature of methoxy-MA but showed that the "*cholesteroid nature of MAs seems to depend on the ability of the AMAA to recognize the trans-keto MA subtype*".[27]

Every study that involves the use of free MAA for serodiagnosis of TB uses phosphatidylcholine (PC, a liposome) as the solubilizing agent. Liposomes are spherical vesicles composed of one or more lipid bilayers, typically made of phospholipid-like phosphatidylcholine,[28] and are used in diverse applications such as drug delivery vehicles for nutrients and pharmaceuticals, signal enhancers in diagnostics, adjuvants in vaccines, solubilizers for various compounds, and support matrices in biochemistry.[29] However, the impact of PC on the cholesterol−MAA interaction and hence the accuracy of diagnosis have not been investigated.

To our knowledge, all the reported works on the use of MAA for the detection of TB involve expensive biosensing fabrication techniques, such as the use of gold plates for surface plasmon resonance (SPR) technique[12] or gold electrodes modified with self-assembled monolayer (SAM).[27] To meet most of the WHO's ASSURED criteria (i.e., Affordability, Sensitivity, Specificity, User-friendliness, Robustness, Equipment-free, and Deliverability) for developing point-of-care (PoC) diagnostic devices, new sensing platforms are needed. Carbon materials, such as activated carbons (ACs), are easily available and more affordable than gold plates and thus can meet some of the ASSURED criteria for PoC devices. For example, the physicochemical properties of AC are expected to allow for efficient encapsulation of the MAA for TB detection.

In this work, therefore, we used AC as a platform for the encapsulation of MAA for the electrochemical detection of TB in HIV-positive sera. In addition, we employed both electrochemical techniques and theoretical (Density Functional Theory, DFT) calculations to investigate the interactions involving the three components (cholesterol−mycolic acid−phosphatidylcholine interactions) and their impact on the detection of TB antibodies in human serum. Our results clearly show that cholesterol interacts with MAA, but even more strongly with PC/MAA.

EXPERIMENTAL SECTION

Materials and Procedure. Saponin and Mycolic acid were purchased from Sigma. *N*,*N*-Dimethylformamide (DMF) was purchased from Applied Biosystems (a division of PerkinElmer, Great Britain) and was dried and distilled within hours/days before use. Phosphatidylcholine (PC) was obtained from Sigma. Potassium chloride (KCl), sodium chloride (NaCl), potassium dihydrogen phosphate (KH_2PO_4), ethylenediaminetetraacetic acid (EDTA), sodium phosphate (Na_2HPO_4), and sodium azide (NaN_2) used for preparing the buffer (PBS/AE) were purchased from Sigma. Potassium ferricyanide ($K_4Fe(CN)_6$) and sodium hydroxide (NaOH) were obtained from Biozone chemicals. Potassium ferrocyanide ($K_3Fe(CN)_6$) was purchased from B.O. Jones Ltd. Ethanol and sulfuric acid (H_2SO_4) were purchased from SAARCHEM. Commercially available activated carbon was used in this work.

Phosphate-buffered saline containing sodium azide (0.025%, m/v) and 1 mM EDTA (PBS/AE, pH 7.4) was prepared with appropriate amounts of Na_2HPO_4 (7.5 mM), KH_2PO_4 (1.5 mM), NaCl (0.14 M), and KCl (2.5 mM). The pH of the buffer was adjusted to 7.4 with 1 M sodium hydroxide (NaOH). Ultrapure water of resistivity better than 18.2 MΩ cm was obtained from a Milli-Q Water System (Millipore Corp., Bedford, MA, USA) and was used throughout for the preparation of solutions.

Liposomes were prepared consisting of only a PC/$CHCl_3$ solution. The PC/$CHCl_3$ contents in an amber glass vial were initially vortexed to ensure thorough mixing and then dried at 85 °C for about 10 min. Liposome formation was induced by addition of 2 mL of saline (0.9% NaCl) and placing in a hot plate at 85 °C for 20 min, with vortexing every 5 min. The liposomes were then ultrasonicated for 24 h at 40 °C. Subsequently, the liposomes were divided into 200 μL aliquots, dried in an oven at 60 °C, and stored at −24 °C until ready for use. Before use, the liposomes were reconstituted with 2 mL of PBS/AE (pH 7.4), heated at 85 °C for 20 min, and then ultrasonicated as before. The final liposome concentration was 500 μg/mL.

Human sera consisted of unused samples from tuberculosis and Human Immunodeficiency Virus-positive (TB^+/HIV^+) and one tuberculosis and Human Immunodeficiency Virus-negative (TB^-/HIV^-) as a control, which were part of a collection for an approved study ("Genotypic and Phenotypic diversity of mycobacterium tuberculosis strain in patients with concomitant pulmonary and extra-pulmonary infection") and were selected from the National Health Laboratory Services (NHLS)−Tshwane Academic Division General Medical Wards of the Steve Biko Academic Hospital, Tshwane (South Africa). Since

https://doi.org/10.1021/acsomega.5c00904
ACS Omega 2025, 10, 50813−50824

this study involved the use of human sera, ethical clearance approvals were acquired before the commencement of the study from both the Ethics Committee of the Faculty of Natural and Agricultural Sciences (NAS) as well as the Human Research Ethics Committee of the Faculty of Health Sciences, University of Pretoria. Figure S1 shows the synthesis procedure for integrating activated carbon with mycolic acid. In a polystyrene cup, mycolic acid antigen (2 mg) and activated carbon (0.5 mg) (in a ratio of 1 activated carbon:4 mycolic acid) were dissolved in 5 mL PBS/AE containing saponin (1.5 mg/mL PBS/AE). This solution was ultrasonicated for 24 h at 40 °C. Subsequently, the solution was dried on a hot plate at a very low temperature and stored at room temperature until ready for use.

Physico-Chemical Characterization. The structure and morphologies of the Activated Carbon (AC) and activated carbon-mycolic acid (AC−MA) used in this work were characterized using X-ray diffraction (XRD), X-ray photoelectron spectra (XPS), scanning electron microscopy (SEM), Raman, and Brunauer−Emmett−Teller (BET) for the activated carbon (Table S1) and Fourier transform infrared spectroscopy as summarized in the Supporting Information. The AC−MA composite was fabricated as described in Figure S1 by simply dissolving MAA and AC in PBS/AE containing saponin, ultrasonicating for 24 h at 40 °C, and drying out the solution on a hot plate.

Electrochemistry and Procedures. Electrochemical experiments were conducted at room temperature ((25 °C) using an Autolab Potentiostat PGSTAT 100) (Eco Chemie, Utrecht, The Netherlands) driven by version 4.9 of GPES, and FRA software version 4.9 was used for carrying out the electrochemical experiments. Glassy carbon electrode (GCE, diameter = 3.0 mm, BAS) with or without modification with the sensing molecules was used as the working electrode; Pt rod and Ag/AgCl (3 M KCl) were used as the counter and reference electrodes, respectively. The electrolyte solution was a PBS/AE solution of the redox probe (i.e., 1 mM $K_4Fe(CN)_6/K_3Fe(CN)_6$ (1:1) mixture containing 0.1 M KCl). Before each experiment, the electrolyte solution was deaerated with pure nitrogen. Electrochemical impedance spectroscopy (EIS) experiments were performed at the equilibrium potential ($E_{1/2}$) redox probe$^-$ (~0.26 V vs AglAgCl, 3 M KCl) between 10 mHz and 10 kHz using a 5 mV rms sinusoidal modulation. The mechanism of detection of mycolic acid antigen−antibody interaction (Figure S2) is described in the Supporting Information.

Electrode Modification as an Immunosensor. In a polystyrene cup, 1.0 mg of Activated carbon integrated with mycolic acid was dissolved in 5 mL of dry DMF containing 100 μL of Nafion. This solution was then ultrasonicated for 24 h at 40 °C. Subsequently, 10 μL of this solution was dropped on a bare glassy carbon electrode (GCE, diameter = 0.0707 cm^2) and then allowed to dry in an oven at 60 °C and the surface was characterized with EIS and CV using PBS/AE (pH 7.4) containing the redox probe.

Electrochemical Detection of Mycolic Acid Antigen−Antibody Interaction. HIV^+/TB^+ and HIV^-/TB^- human sera were suitably diluted (0, 50, 100, 200, 250, and 300 μL) in PBS/AE (pH 7.4)-diluted empty liposomes. For control studies, a similar procedure was used with liposomes containing MA. Prior to conducting the CV and EIS experiment in a test solution of 0.1 M $[Fe(CN)_6]^{4-}/[Fe(CN)_6]^{3-}$ (PBS/AE, pH 7.4) at a bias potential of 0.27 V (vs AglAgCl, sat'd KCl), to get rid of any physically attached species, the modified electrode (working electrode) was rinsed in a lot of PBS/AE (pH 7.4) after being incubated in the proper serum solution for 10 min. Safety Note: All glassware in contact with human sera (both TB positive and negative) were sterilized by autoclaving for 20 min at 115 °C after use. Waste solutions were carefully collected and sterilized before disposal. All students and lecturer who were working in the laboratory where the antibody−antigen interaction analysis experiments were conducted were vaccinated against hepatitis B.

Density Functional Theory (DFT) Simulation Details. Density Functional Theory (DFT) studies were carried out with the supercomputational facilities at the Centre for High Performance Computing (CHPC, Cape Town, South Africa) utilizing the BIOVIA Material Studio. For details of the molecular structures of the PC, MA, and PC/MA and others, please see the Supporting Information (including Figure S3).

RESULTS AND DISCUSSION

Physico-Chemical Properties of Carbon-Encapsulated Mycolic Acids. The HRSEM images of the AC and AC−MA show porous AC (Figure 1A) and plate-like morphology of the AC−MA (Figure 1C), while the corresponding EDX (Figure 1B and D, respectively) confirms the presence of Sodium Chloride (NaCl) salt. The SEM/EDX map (Figure 1E) confirms the presence of the various elemental compositions of the AC−MA.

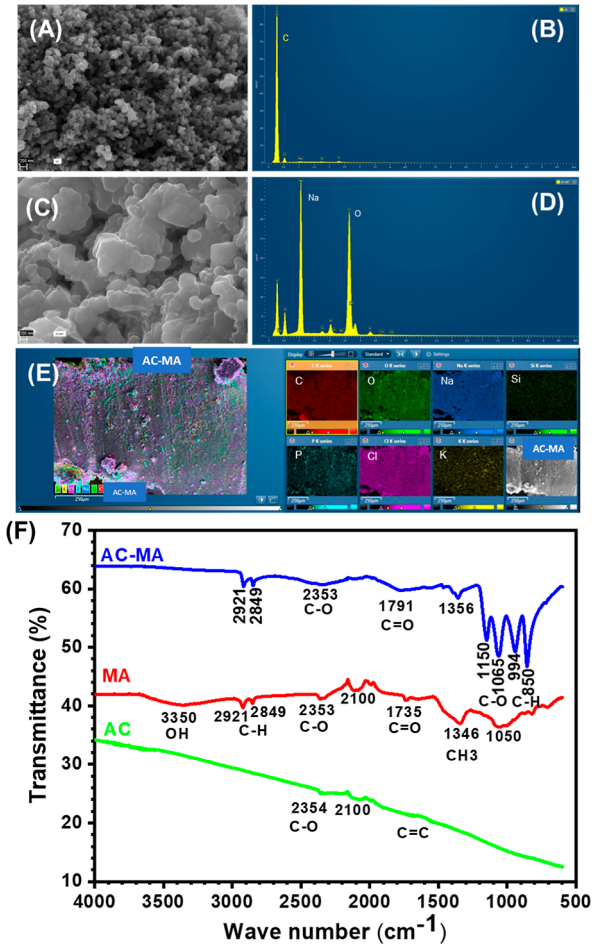

Figure 1. Comparative SEM images of the (A) Activated Carbon and (C) Activated Carbon-mycolic acid antigens and their corresponding EDX images in (B) and (D), respectively; (E) SEM/EDX map of the various elemental compositions of the AC−MA; (F) comparison of the FTIR of the AC, MA, and AC−MA.

https://doi.org/10.1021/acsomega.5c00904
ACS Omega 2025, 10, 50813−50824

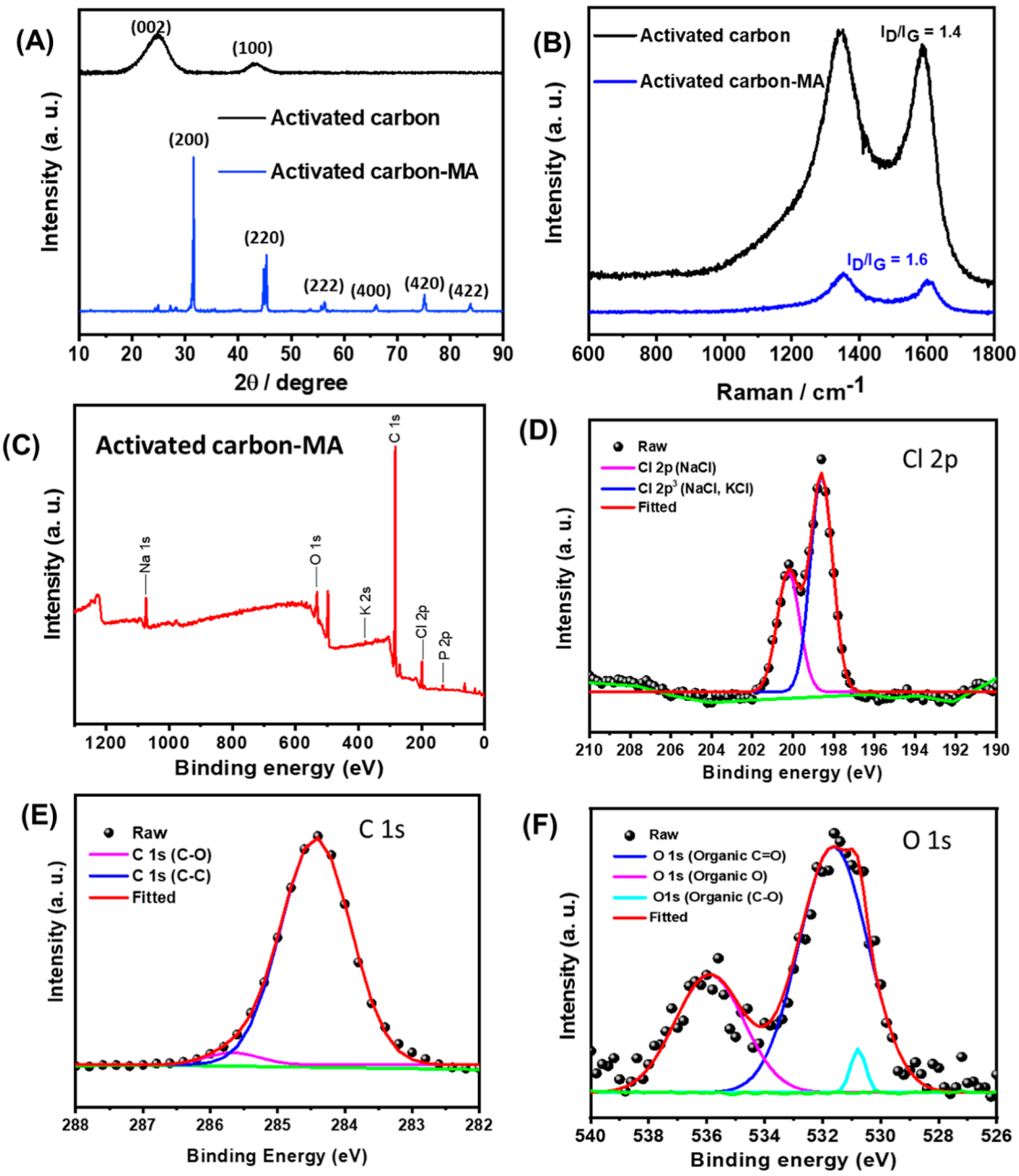

Figure 2. X-ray diffraction pattern (A), Raman spectra (B), and XPS survey (C) of activated carbon-encapsulated mycolic acid (AC−MA). Deconvoluted XPS spectra of the Cl 1s (D), C 1s (E), and O 1s region (F) of the AC−MA.

Nitrogen gas adsorption−desorption experiments and Brunauer−Emmett−Teller (BET) analysis for the AC confirm a high surface area (622.2057 m^2/g) and high microporous volume (0.050566 cm^3/g) with an average pore width of 2.31439 nm (see Table S1).

Figure 1F shows the infrared spectra of AC, MA, and AC−MA after drying at low temperatures (40−50 °C) to retain their structural integrity. The intensities and positions of the absorption peaks are significantly different. The MA spectrum shows a strong broad peak around 3350 cm^{-1} ascribed to O−H stretching vibration of the hydroxyl group of the mycolic acid. The bands in the 2921−2849 cm^{-1} region are due to the C−H stretching in methyl and methylene (CH_3 and CH_2) groups, representing the alkyl chains and the methoxy group ($-OCH_3$) of the mycolic acid. The band around 2353 cm^{-1} is ascribed to the C−O stretching. The broad band at 2100 cm^{-1} is due to polarizable hydrogen-bonded continua.[30]

The band at 1735 cm^{-1} is due to the vibration of the carbonyl and keto groups (C═O), while the weak band in the 1690−1620 cm^{-1} region is due to the C═C vibration. The fingerprint region (1300−1070 cm^{-1}) shows the C−O and C−H bands of the methoxy group ($-OCH_3$). As expected, the C−O stretching vibration of the methoxy group is usually observed as a sharp, intense peak in this region. As observed, the AC spectrum shows weak peaks of the C═C, C−O, and polarizable hydrogen-bonded system. Interestingly, however, the AC−MA spectrum is slightly different from those of the MA and AC by showing (i) no detectable O−H band and (ii) broad fingerprints but well-defined fingerprints in the 1300−1070 cm^{-1} region for the C−O and C−H vibrations. Thus, the difference in the AC−MA from those of the AC and MA is an indication that AC was

https://doi.org/10.1021/acsomega.5c00904
ACS Omega 2025, 10, 50813−50824

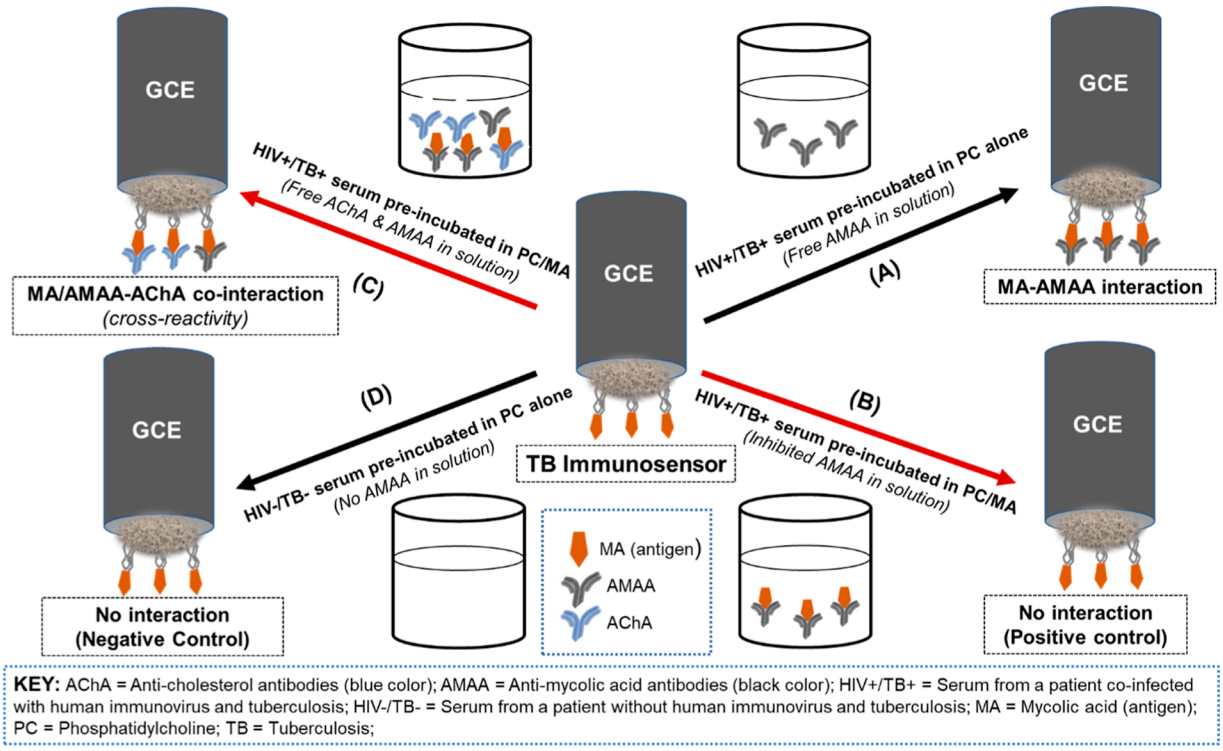

Figure 3. This is the author's hypothesis for the detection of mycolic acid antigen−antibody interaction for TB detection based on literature precedents.[12,26,27] This hypothesis is tested both experimentally and theoretically (DFT studies).

successfully coupled with the MA. However, such coupling of the AC with MA is most likely to be due to the van der Waals interactions, which are weak and distance-dependent forces of attraction and repulsion between carbon, hydrogen, and oxygen atoms existing between the two molecules.

Powder XRD patterns of the AC (Figure 2A) are consistent with porous carbon materials, with characteristic peaks at the 2θ values of 25.2° and 43.8° ascribed to the *hkl* of (002) and (100), respectively.[20] However, unlike AC, the AC−MA composite shows highly crystalline peaks due to the presence of the NaCl salt used in the preparation methods from PBS/AE (pH 7.4). This means that the highly crystalline NaCl suppressed the carbon peaks of the AC−MA. Figure 2B compares the Raman spectra of the AC and the AC−MA electrode materials. The presence of carbon in both the AC and AC−MA is confirmed by the Raman peak associated with the carbon D mode (1350 cm^{-1}) and G mode (1590 cm^{-1}).[31,32] The I_D/I_G ratios are 1.4 and 1.6 for AC and AC−MA, respectively. This result means that in the experimental conditions employed in this work, AC−MA is more defective than AC alone. The presence of defects further confirms the successful integration of MA into AC. Figure 2C is the XPS survey scan for the AC−MA, showing all of the expected elements (Na, Cl, O, P, C) from both the precursor and solution materials involved in its preparation, which corroborates the EDX data (Figure 1E). The deconvoluted spectrum of Cl (Figure 2D) indicates its source as NaCl. The deconvoluted O 1s spectrum (Figure 2E) comprises organic C═O and C−O species, while the deconvoluted spectrum of C 1s (Figure 2F) is mostly related to the organic C−C bonds, all arising from MA and AC.

Hypothesis of TB Detection: Experimental Design and Rationale. Benadie et al., 2008, and Ranchod et al., 2018, reported the antigenicity and cholesteroid nature of mycolic acid that showed the following:[26,27]

i Antibodies in tuberculosis (TB) patient sera respond differently toward the three MA classes and were reported to cross-react with cholesterol (i.e., cholesterol behaves like an antigen just like the MMA).

ii Mycobacterial MA (MMA) cross-reacts with cholesterol.

iii The cholesteroid nature of MMA seems to be dominated by the trans-keto MA subclass.

iv TB patients produce antimycolic acid antibodies (AMAAs).

v The AMAA levels are maintained in sera of HIV-infected TB patients regardless of a declining $CD4^+$ T cell count.[11,27] This enables a biomarker test based on detection of AMAA to detect active TB disease regardless of the HIV status of the patient. In the past decade, there has been a rise in the incidences of tuberculosis partly owing to coinfection with HIV. Thus, there has been an urgent need for the detection of TB in the presence of HIV-positive coinfected patients.[33]

vi Although AMAAs are known to exist in TB patients, the antigen moiety of MAs that is recognized by the antibodies is not known and the molecular basis that governs MA-specific Ab-MA interactions is not well understood.

Based on the literature precedents as summarized above, i.e., (i)−(vi), a hypothesis for the electrochemical detection of TB in both HIV-positive and HIV-negative patients has been proposed as shown in Figure 3.

TB capacitive immunosensor was interrogated using the conventional redox probe, the reaction mechanism of which (i.e., lock-and-key suppression) is well described in the literature (also see Figure S2).[23,33] In this work, the TB capacitive immunosensor was constructed, with exposed mycobacterial MA (antigen) to interact with antimycolic acid antibodies

https://doi.org/10.1021/acsomega.5c00904
ACS Omega 2025, 10, 50813−50824

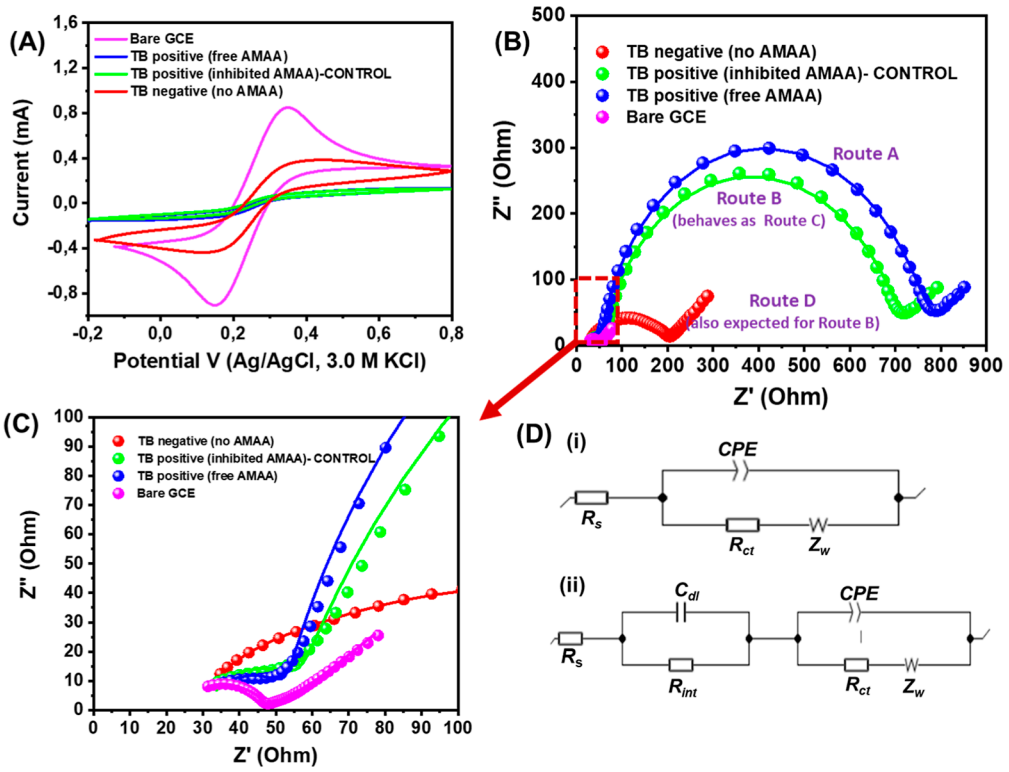

Figure 4. CV plots (A) and EIS evolutions (B,C) obtained for the GCE−AC−MA after it was exposed to a TB-negative and -positive patient serum after preincubation with empty or mycolic acid-containing liposomes. (D) Electrical equivalent circuit model is used to fit the impedance spectrum. Note: The symbols represent experimental data, while solid lines are fitted curves using electrical equivalent circuits.

Table 1. CV and EIS Parameters for the GCE and GCE-Modified TB Immunosensor in Different Serum Solutions

measured parameter	bare GCE	TB negative (control)	TB positive (control)	TB positive (real sample)
		CV Data		
E_{pa}/V	0.34	0.42	0.67	0.68
E_{pc}/V	0.16	0.14	−0.11	−0.11
ΔE_p/V	0.18	0.28	0.78	0.79
$E_{1/2}$/V	0.25	0.28	0.39	0.40
I_{pa}/μA	0.92	0.38	0.16	0.15
I_{pc}/μA	−0.96	−0.43	−0.18	−0.16
I_{pa}/Ipc	0.96	0.88	0.89	0.94
		EIS Data		
R_s/Ω	15.29 ± 3.21	23.78 ± 0.66	31.80 ± 0.70	31.54 ± 0.58
C_{dl}/μF		9.28 ± 2.10	2.46 ± 0.19	2.40 ± 0.17
R_{int}/Ω		6.71 ± 1.52	22.77 ± 0.84	19.91 ± 0.63
CPE/μF s(n−1)	0.053 ± 0.004	0.107 ± 0.018	17.01 ± 1.03	24.86 ± 0.98
n	0.61	0.56	0.85	0.89
R_{ct}/Ω	34.20 ± 3.36	174.90 ± 2.40	651.00 ± 7.28	711.00 ± 5.96
Zw/Ω s−0.5	0.032 ± 0.001	0.036 ± 0.001	0.035 ± 0.005	0.033 ± 0.004
phase angle/°	−15	−26	−50	−55
i°/A	3.44×10^{-4}	6.73×10^{-5}	1.81×10^{-5}	1.65×10^{-5}
k_{het}/cm s^{-1}	2.52×10^{-8}	4.93×10^{-9}	1.32×10^{-9}	1.21×10^{-9}

(AMAAs). Three types of responses by the redox probe should be expected:

- Route A: If the TB immunosensor is incubated in the serum of a patient coinfected with HIV and TB (i.e., HIV^+/TB^+ serum) which was previously incubated in PC alone, it is expected that the free AMAA present in the serum will interact with the exposed MA antigen. Ideally, electrochemistry should respond to this lock-and-key interaction by a suppressed electron transport of the redox probe.
- Route B: If the TB immunosensor is incubated in a HIV^+/TB^+ serum, previously incubated in PC and MA, it is expected that any AMAA present will have reacted with the MA antigen (inhibited AMAA in solution); thus, the exposed MA antigen will have no AMAA to interact with, so ideally no electrochemical response should be expected.

https://doi.org/10.1021/acsomega.5c00904
ACS Omega 2025, 10, 50813−50824

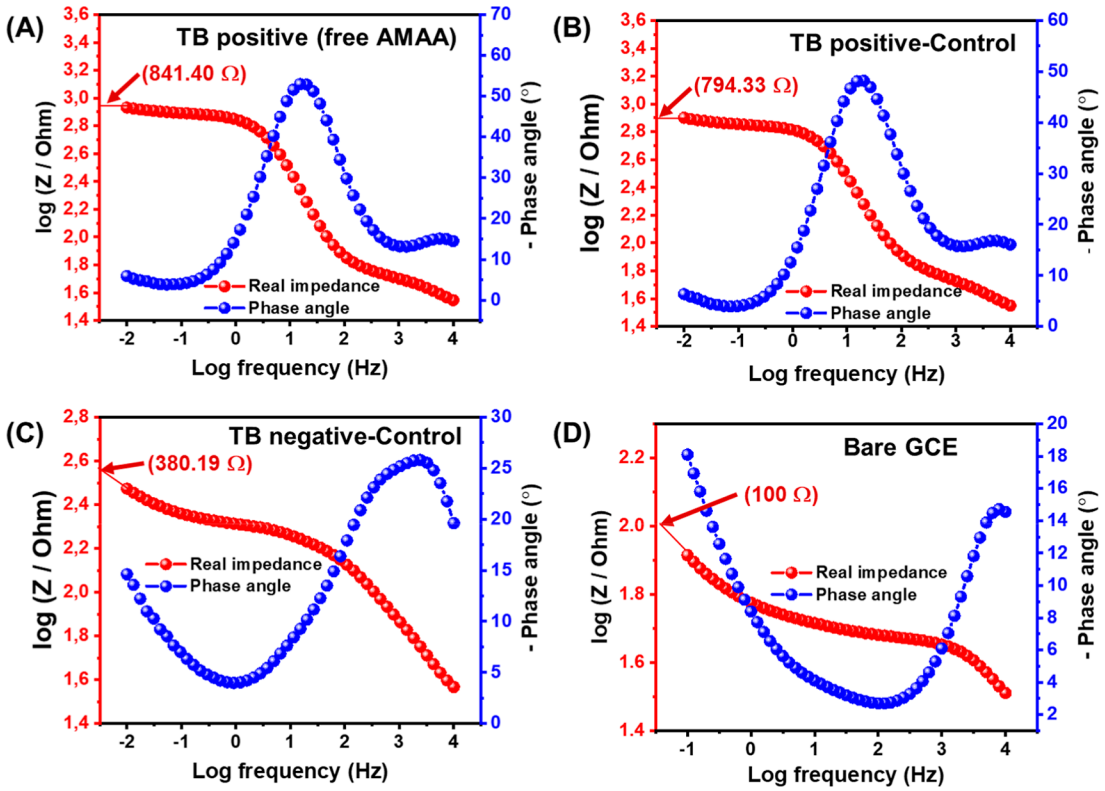

Figure 5. EIS Bode plots for the GCE−AC−MA after it was exposed to (A) TB-positive (free AMAA, route A), (B) TB-positive control (route B), (C) TB-negative control (route D), and (D) bare GCEs.

- Route C: If the TB immunosensor is incubated in an HIV^+/TB^+ serum preincubated in PC/MA, considering the cholesterol nature of MA, then the free AMAA and free anticholesterol antibodies (AChAs) present in the solution will compete with the exposed MA antigen of the immunosensor, leaving behind some free AChA and AMAA in solution that can still bind to the MA antigen of the immunosensor. Ideally, electrochemistry should respond to this lock-and-key interaction brought about by the AChA and AMAA, which will be observed by suppressed electron transport of the redox probe.
- Route D: If the TB immunosensor is incubated in a HIV^-/TB^- serum preincubated in PC alone, there is no free AMAA present in the serum to interact with the exposed MA antigen of the immunosensor. Ideally, no electrochemical response should be expected.

Testing the Hypothesis: Electrochemical Detection of TB. The TB immunosensor was incubated in different solutions (as shown in Figure 3, Routes A−D) and then tested in the redox probe (0.1 M $[Fe(CN)_6]^{4-}/[Fe(CN)_6]^{3-}$ (PBS, pH 7.4)) using both CV and EIS methods. As shown from the CV evolutions (Figure 4A and Table 1), the resistance to electron transport, demonstrated by the peak-to-peak separation (ΔE_p), decreases as follows: GCE-immunosensor (HIV^+/TB^+, route A) (0.79 V) ≈ GCE-immunosensor (HIV^+/TB^+ control, route B) (0.78 V) > GCE-immunosensor (HIV-/TB-control, route D) (0.28 V) > bare GCE (0.18 V). Ideally, the control experimental routes B and D are expected to show similar voltammetric responses (i.e., little or no inhibition to electron transport expected). Interestingly, while route A is expected to inhibit electron transport (due to the presence of free AMAA), route B (no free AMAA to interact with the TB immunosensor) is not expected to give a similar behavior. This finding clearly suggests that route C is in operation rather than route B, meaning that free AChAs (and free AMAA still present in solution) bind to the MA antigen of the TB immunosensor, confirming the literature reports that cholesterol is usually present in the blood of HIV^+/TB^+ patients[36] as well as the established cholesteroid nature of the MA.[26,27,35]

To complement the CV data, EIS experiments were also conducted for the TB immunosensors interacting with the different serum solutions to extract their electro-transfer kinetics. Figures 4B and C compare the Nyquist plots for the interaction of the TB immunosensor with the various serum solutions. The EIS data are visualized as Nyquist and Bode plots. The Nyquist plots were satisfactorily fitted with the Randles equivalent electrical circuit (EEC) for the bare GCE, Figure 4D(i), and combined with Randles with one Voigt EEC (for the GCE-modified TB immunosensor, Figure 4D(ii)). These EECs comprise the electrolyte resistance (R_s), interfacial resistance (R_{int}) associated with the IR drop and the corresponding capacitance of the interfacial layer (C_{dl}), electron-transfer resistance (R_{ct}), constant phase element (CPE), and Warburg-type diffusion impedance (Z_w) associated with the diffusion of the ions of the redox probe. The impedance associated with the CPE (Z_{CPE}) can be defined as shown in eq 1:[34,36−40]

$$Z_{CPE} = \frac{1}{Q(jw)^n} \quad (1)$$

where Q is a constant arising from the electrode−electrolyte interface, $j = \sqrt{-1}$, ω represents the radial frequency, n is the slope of the plot of log Z against log F (i.e., Bode plot) with values between −1 and +, i.e., $-1 \le n \le 1$: when $n = 0$, it means that the CPE is a pure resistor; when $n = 1$, the CPE is a pure

https://doi.org/10.1021/acsomega.5c00904
ACS Omega 2025, 10, 50813−50824

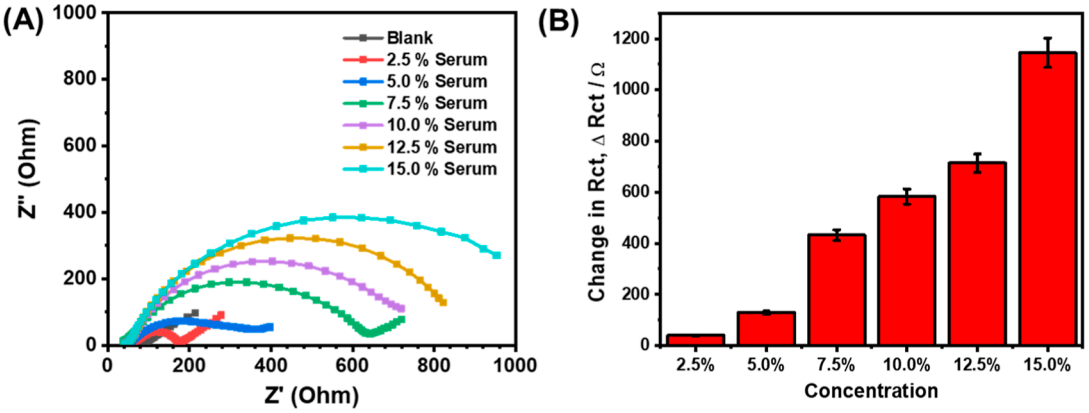

Figure 6. Typical Nyquist plots (A) and bar chart (B) of the various dilutions (2.5−15%) of TB-positive/HIV-positive patient serum preincubated using the TB capacitive electrochemical immunosensor.

capacitor; when $n = -1$, the CPE is an inductor; and when $n = 0.5$, the CPE is equivalent to the Warburg impedance (Z_w). From Table 1, the total series resistance ($R_s + R_{int} + R_{ct}$) decreases as follows (within the error limits, approximately): GCE-immunosensor (HIV^+/TB^+, route A) (763 Ω) > GCE-immunosensor (HIV^+/TB^+ control, route B) (686 Ω) > GCE-immunosensor (HIV^-/TB^- control, route D) (205 Ω) > bare GCE (50 Ω).

The EIS result follows the same trend as the ΔE_p except that the EIS data is more sensitive by separating the signals more clearly than the CV. However, the interpretations for both CV and EIS are the same. The real positive serum (route A) behaved as expected. Negative control (route D) behaved as expected. Positive control (route B) was expected to behave as its corresponding negative control (route D), but this was not the case. Instead, the positive control (route B) showed a signal that is near the real positive serum (route A). The result confirms that route C (i.e., cross reactivity due to the cholesteroid nature of the MA) is in operation rather than route B (positive control), which agrees with the literature.

The CPE in the fitting parameter suggests that the electrode surfaces are porous and rough. The "n" values of the CPE are between 0.56 and 0.89, indicating a mixed reaction mechanism of pseudocapacitance. The Z_w values are almost the same for all the surfaces which implies that ionic diffusion/transport is the same for the electrodes, while electronic transport (R_{ct}) is not. From the EIS data, we can determine the exchange current (i_0) and the rate constant for the heterogeneous electron transfer (k_{het}) using eqs 2 and 3:[41−43]

$$i_0 = \frac{RT}{nFR_{ct}} \tag{2}$$

$$k_{het} = \frac{i_0}{nFA} \tag{3}$$

where A is the geometric surface area of the GCE (0.0707 cm^2), R is the gas constant (8.314 J K^{-1} mol^{-1}), T is the Kelvin temperature (273 K), and n is the number of electrons transferred (2 for the redox probe used in this work), while F is the Faraday constant (96,485.33 C mol^{-1}). The higher the values of i_0 and k_{het} are, the better the electron transport properties. From Table 1, it can be observed that k_{het} follows the same trend as the R_{ct}: bare GCE (2.52×10^{-8} cm s^{-1}) > GCE-immunosensor (HIV^-/TB^- control, route D) (4.93×10^{-9} cm s^{-1}) > GCE-immunosensor (HIV^+/TB^+ control, route B) (1.32×10^{-9} cm s^{-1}) > GCE-immunosensor (HIV^+/TB^+, route A) (1.21×10^{-9} cm s^{-1}), meaning that electron transfer becomes more sluggish as one moves from the bare GCE to the real infected sample.

From the Bode plots, log Z vs log f vs phase angle (Figure 5), we observe further the phase angles (i.e., phase angle (ϕ) vs log f) are less than the 90° expected of an ideal capacitive behavior, confirming the pseudocapacitive behavior. Importantly, the real impedance also decreases as follows: GCE-immunosensor (HIV^+/TB^+, route A, Figure 5A) (841.40 Ω) > GCE-immunosensor (HIV^+/TB^+ control, route B, Figure 5B) (794.33 Ω) > GCE-immunosensor (HIV^-/TB^- control, route D, Figure 5C) (380.19 Ω) > bare GCE (Figure 5D) (100 Ω), meaning that electron-transfer becomes more sluggish as one moves from the bare GCE to the real infected sample.

Contrary to expectations, the preincubation of the GCE−TB immunosensor in empty liposomes (PC alone) or mycolic acid-containing liposomes (PC/MA) when testing the TB positive sera (routes A or B) gave an almost identical electrical resistance (Table 1 and Figure 4). This unexpected behavior of route B may be attributed to the presence of cholesterol in the serum sample (route C), confirming what others have observed using a nonelectrochemical method.[26,27] In other words, rather than observing route B, route C was observed. This means that cholesterol might cross-react not only with MA but also with liposomes. It is against this background that the preincubation of the GCE−TB immunosensor in liposomes containing mycolic acid (i.e., PC/MA) was discontinued in subsequent electrochemical experiments in this PhD thesis. Thus, electroanalytical detection at different concentrations of TB positive sera was focused on route A (i.e., liposomes alone).

Concentration Studies. It should be noted that mycolic acid (MA) is a key antigen for detecting TB antibodies, although antimycolic acid antibodies (AMAAs) have not yet been isolated; hence, it is not commercially available, which makes it impossible to quantitatively determine its concentration in human serum. Thus, in this work, we have to indirectly determine the ability of the immunosensors for TB detection by diluting the human sera acquired from the hospital (the ethical clearance certificate duly obtained from the University of Pretoria). Based on the CV and EIS findings, the concentration studies of the TB-positive sera were investigated using empty liposomes (route A). Considering the high sensitivity of EIS over CV, EIS was used to check the response of the immunosensor (GCE−AC−MA) toward different dilutions of

https://doi.org/10.1021/acsomega.5c00904
ACS Omega 2025, 10, 50813−50824

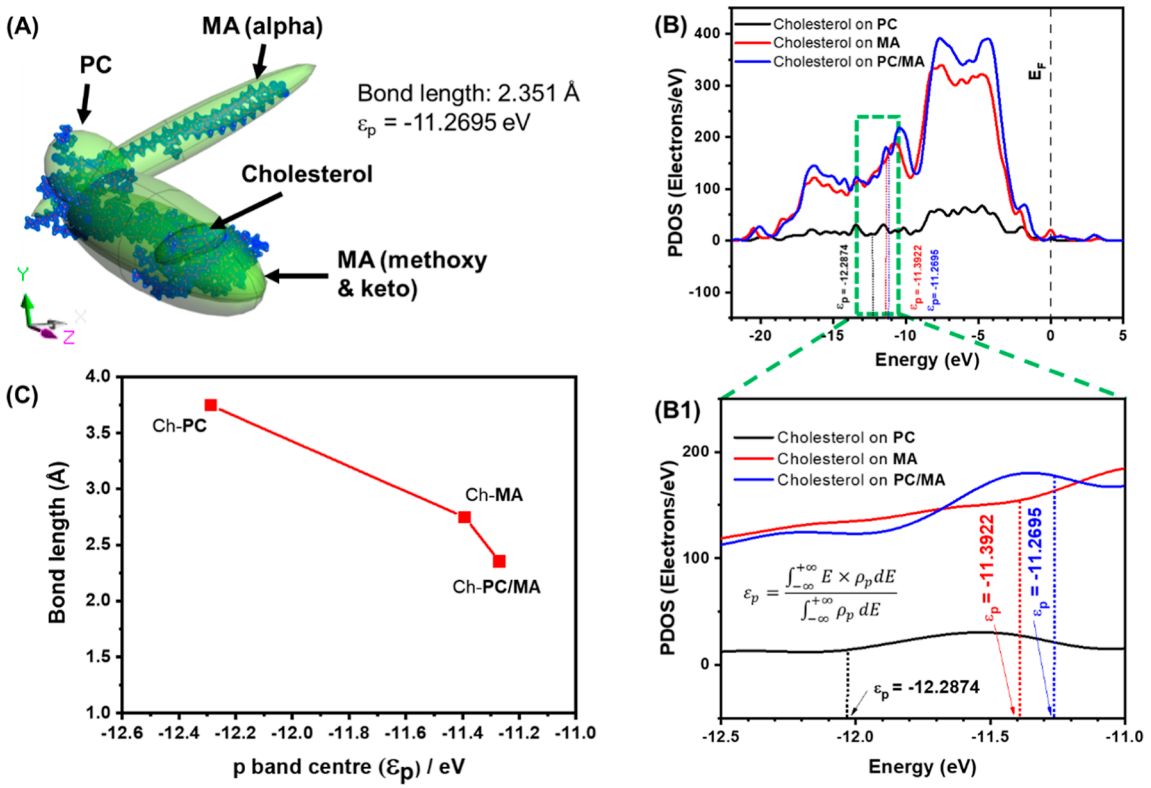

Figure 7. (A) Calculated model of the Ch−PC/MA interaction, (B) projected partial density of states (PDOS) of the interaction of cholesterol with each of the organic molecules (PC, MA, and PC/MA) showing the p-band centers. (B1) The zoomed-in section of the p-band centers. The Fermi level is set to 0 eV and shown as the gray dashed line. The p-band centers are represented by the black, red, and blue dotted lines. (C) Plots of the bond length against the p-band center for the interaction between cholesterol (Ch) and PC, MA, and PC/MA.

TB-positive sera (2.5−15%). Figure 6A shows typical Nyquist plots obtained after immersing the TB electrochemical immunosensor in different concentrations of the human sera from HIV^+TB^+ patients. Using the EIS data, the concentration study results are represented as a bar chart for a range of serum dilutions (Figure 6B).

The change in the total charge transfer resistance ($\Delta R_{ct}/\Omega$) for each concentration of the human sera was calculated from eqs 4 and 5 below:[44,45]

$$\Delta R_{ct}/\Omega = R_{Ag-Ab} - R_{Ag} \quad (4)$$

$$\Delta I_p/\mu A = I_{p(blank)} - I_{p[conc]} \quad (5)$$

where R_{Ag} is the electron transfer resistance prior to incubation of the electrochemical immunosensor in the serum, while R_{Ag-Ab} is the electron transfer resistance after the GCE−AC−MA electrode is incubated in the serum. The different serum samples showed increased blockage of diffusion as the concentration increased, indicating the binding of the anti-MA antibodies (AMAAs) in the sera and the interaction of these antibodies with the immobilized mycolic acid antigen (MAA), thus confirming that the new TB electrochemical immunosensor can be used to detect different concentrations of TB antibodies in TB-positive patients. EIS technique is becoming commercially available in miniaturized electrochemical devices, which is promising for the future development of point-of-care diagnostic devices.

Testing the Hypothesis: Theoretical Insights from DFT Studies. From the preceding section, we observed from electrochemical data that the immunosensor surface (i.e., MA antigen) interacts with the TB antibody in serum solution containing PC alone (route A) and PC mixed MA (routes B and C). The fact that route C is considered as having cross-reactivity with cholesterol raises some important questions that need some answers. Such questions include:

1 Can PC interact with cholesterol (Ch) and, if yes, to what extent?

2 Can PC/MA interact with cholesterol (Ch) and, if yes, to what extent?

To answer the above questions, we embarked on theoretical (DFT) simulation of the interactions between Ch and PC, Ch and MA, and Ch and PC/MA (Figure S4 and Table S2). It is very interesting to observe in Figure S4 that Ch specifically interacts with the most antigenic parts of the MA (i.e., methoxy and keto groups) but strongly distances itself from the alpha-MA part. This specific interaction may interfere or limit the antigenic tendencies of the methoxy/keto groups toward the detection of the AMAA in TB sera, hence, the cross-reactivity and poor accuracy of TB detection. Also, the finding shows the "neutrality" of alpha-MA toward cholesterol. PC binds at the base where the three MA parts meet.

Comparing the partial density of states (PDOS) (Figure S5), it was observed that the interaction with cholesterol increases as follows: Ch−PC < Ch−MA < Ch−PC/MA. This result means that the interactions arising from Ch−MA and Ch−PC/MA are accompanied by higher charge domination than that of the Ch−PC interaction. This interaction benefits conductivities of Ch−MA and Ch−PC/MA interactions. The dipole moment indicates the difference in the electronegativities of the bonded atoms, the larger the dipole moment value, the larger the difference in electronegativities of the bonded atoms.

https://doi.org/10.1021/acsomega.5c00904
ACS Omega 2025, 10, 50813−50824

In electrochemistry, the "p-band center" is a crucial descriptor of catalysis as it allows one to understand and predict how strongly or weakly a material (an electrode material or catalyst) interacts with a reactant or its intermediates. A high negative value (i.e., far away from the Fermi energy level) indicates weak interaction, while a low negative value (i.e., closer to the Fermi energy level) indicates strong interaction, potentially resulting in higher catalytic activity. From the PDOS (Figure S5), we observe that only the s- and p-bands are present, with the p-band as the dominant band. This should be expected as the molecules investigated in this work are organic materials containing nonmetallic elements C, H, O, N, and P. The interaction of cholesterol with the PC, MA, and PC/MA substrates can be characterized by the p-band center of PDOS. The p-band center (ε_p) was calculated considering both the unoccupied and occupied orbitals according to the following equation:

$$\varepsilon_p = \frac{\int_{-\infty}^{+\infty} E \times \rho_p dE}{\int_{-\infty}^{+\infty} \rho_p dE} \quad (6)$$

where ρ_P and E are the PDOS and energy of the p-states, respectively.

Figure 7A exemplifies a typical model of the cholesterol interaction with the PC/MA, while Figure 7B shows the projected partial density of states (PDOS) of the interaction of cholesterol with each of the organic molecules investigated (i.e., PC, MA, and PC/MA) showing their calculated p-band centers. The location of the p-band center is the result of atomic orbital hybridization, i.e., the hybridization of the p-state atoms of the cholesterol with those of the PC, MA, or PC/MA. The p-band center (ε_p) follows the trends: PC (−12.2874 eV) > MA (−11.3922 eV) > PC/MA (−11.2695 eV), meaning that cholesterol interaction with the PC is the weakest, while that of the PC/MA is the strongest. The interaction of cholesterol on PC allows for the favorable interaction of the antimycolic acid antibodies (AMAAs) of TB to be detected with the mycolic acid (MA) antigen (route A). Also, Table S2 confirms that the cholesterol interaction is more favorable when PC is combined with MA (PC/MA). This high affinity of cholesterol toward PC/MA may confirm the cross-reactivity of cholesterol/cholesterol antibodies and AMAA with the GCE-immobilized MA antigen (as observed for route C), corroborating the cholesteroid nature of the MA.

We further interrogated the possible relationship between the p-band center for the interaction of the cholesterol atoms with PC, MA, and PC/MA atoms and the corresponding bond lengths. Figure 7C depicts the trend where, as the p-band center shifts toward the Fermi level, the bond length gradually decreases. The results show that the shorter the bond length between the adsorbate (i.e., cholesterol (Ch)) and the adsorbent (i.e., PC, MA, and PC/MA), the stronger the p-band center (i.e., strong binding to the atomic nucleus).

CONCLUSIONS

This work is an attempt to advance the electrochemical immunodetection of active TB in HIV-positive patient's serum using a mycolic acid antigen (MAA). The key challenge to the use of MAA in the TB detection protocol is the cross-reactivity of cholesterol (Ch) and anticholesterol antibodies (AChAs) due to the cholesteroid nature of the MAA. In this new study, the cholesteroidal nature of the MAA has been established for the first time with electrochemistry and supported by theoretical (DFT) calculations. Unlike other studies that have not taken cognizance of the possible effect of the conventional liposome (phosphatidylcholine, PC) used in the MAA-based TB detection, we prove that PC indeed interferes with the Ch−MA interactions and hence the TB detection. A novel TB electrochemical immunosensor has been proposed as GCE−AC−MAA and can be tuned to mitigate the cross-reactivity with AChA, hence improved detection of TB. The proposed detection protocol involved preincubating TB serum in liposomes alone (i.e., free AMAA). DFT calculations revealed that cholesterol interacts with MAA (p-band center, ε_p = −11.3922 eV) but more strongly in the presence of both the liposomes and MAA (ε_p = −11.2695 eV). Generally, our theoretical calculations prove that the longer the bond length between cholesterol and the adsorbent (liposome, MAA, or liposome/MAA), the weaker the interaction energy. These findings provide some useful insights that would allow for future improvements in the TB immunodetection strategies.

ASSOCIATED CONTENT

Supporting Information

The Supporting Information is available free of charge at https://pubs.acs.org/doi/10.1021/acsomega.5c00904.

Cartoon representation of the synthesis of activated carbon-encapsulated mycolic acid antigens; fabrication of the TB immunosensor and sensing mechanism described by the cyclic voltammetric evolutions such as the lock-and-key principle; physico-chemical characterization including SEM, XRD, XPS, BET, and FTIR; description of the DFT calculation procedure, including PDOS and p-band centers; molecular structures of mycolic acid and cholesterol; interactions between cholesterol (Ch) and mycolic acids (MA), Ch and MA, and Ch and PC/MA; typical projected partial density of states vs energy of cholesterol adsorbed onto PC, MA, and PC/MA; DFT coordinates that can be accessed with relevant software such as VESTA software; and tables showing characteristics of the activated carbons used in this work as well as summary of the DFT-calculated values of the structural parameters for the adsorption of cholesterol on different molecules (PDF)

AUTHOR INFORMATION

Corresponding Author

Kenneth I. Ozoemena − *Department of Chemistry, University of Pretoria, Pretoria 0002, South Africa; Molecular Sciences Institute, School of Chemistry, University of the Witwatersrand, Johannesburg 2050, South Africa;* orcid.org/0000-0001-7107-7003; Email: Kenneth.ozoemena@wits.ac.za

Authors

Nsovo S. Mathebula − *Department of Chemistry, University of Pretoria, Pretoria 0002, South Africa*

Okoroike C. Ozoemena − *Electrochemical Technology Centre, Department of Chemistry, University of Guelph, Guelph, Ontario N1G 2W1, Canada*

Patrick V. Mwonga − *Molecular Sciences Institute, School of Chemistry, University of the Witwatersrand, Johannesburg 2050, South Africa*

Aderemi B. Haruna − *Molecular Sciences Institute, School of Chemistry, University of the Witwatersrand, Johannesburg 2050, South Africa*

https://doi.org/10.1021/acsomega.5c00904
ACS Omega 2025, 10, 50813−50824

Complete contact information is available at:
https://pubs.acs.org/10.1021/acsomega.5c00904

Notes

The authors declare no competing financial interest.

■ ACKNOWLEDGMENTS

This project was supported by the University of Pretoria and the National Research Foundation of South Africa via the DSI-NRF-Wits SARChI Chair in Materials Electrochemistry and Energy Technologies (MEET) (UID no.: 132739). We thank the Ethics Committee of the Faculty of Natural and Agricultural Sciences (NAS) of the University of Pretoria for approval of this study (ref. No. NAS471/2019) and South Africa's National Health Laboratory Service (NHLS) and the Human Research Ethics Committee of the Faculty of Health Sciences, University of Pretoria, for approval and permission to access "un-used serum identified in subjects of an approved study: Genotypic and phenotypic diversity of mycobacterium tuberculosis strain in patients with concomitant pulmonary and extra-pulmonary infection". We are grateful to late Prof Nontombi Mbelle (PhD), a pathologist of the Department of Medical Microbiology at the Steve Biko Medical Hospital, for her professional advice and support for the project.

■ REFERENCES

(1) Global Tuberculosis Report Bhargava, A.; Bhargava, M. Tuberculosis deaths are predictable and preventable: Comprehensive assessment and clinical care is the key. *J. Clin. Tuberc. Other Mycobact. Dis.* **2020**, *19*, 100155. https://www.who.int/teams/global-tuberculosis-programme/tb-reports/global-tuberculosis-report-2022

(2) Ockenga, J.; Fuhse, K.; Chatterjee, S.; Malykh, R.; Rippin, H.; Pirlich, M.; Yedilbayev, A.; Wickramasinghe, K.; Barazzoni, R. Tuberculosis and malnutrition: The European perspective. *Clin. Nutr.* **2023**, *42* (4), 486−492.

(3) Goletti, D.; Martineau, A. R. Pathogenesis and immunology of tuberculosis. *Essential Tuberculosis*; Migliori, G. B., Raviglione, M. C., Eds.; Springer Nature Switzerland AG: Cham, 2021; pp 20−28.

(4) Olvany, J. M.; Sausville, L. N.; White, M. J.; Tacconelli, A.; Tavera, G.; Sobota, R. S.; Ciccacci, C.; Bohlbro, A. S.; Wejse, C.; Williams, S. M.; Sirugo, G. CLEC4E (Mincle) genetic variation associates with pulmonary tuberculosisin Guinea-Bissau (West Africa). *Infect. Genet. Evol.* **2020**, *85*, 104560.

(5) World Health Organization. *Global Tuberculosis Report 2017*; WHO/HTM/TB: Geneva, Switzerland, 2017.

(6) Uplekar, M.; Weil, D.; Lonnroth, K.; Jaramillo, E.; Lienhardt, C.; Dias, H. M.; et al. WHO's new End TB Strategy. *Lancet* **2015**, *385*, 1799−1801.

(7) Singh, P.; Rameshwaram, N. R.; Ghosh, S.; Mukhopadhyay, S. Cell envelope lipids in the pathophysiology of Mycobacterium tuberculosis. *Future Microbiol.* **2018**, *13*, 689−710.

(8) Ghazaei, C. Mycobacterium tuberculosis and lipids: Insights into molecular mechanisms from persistence to virulence. *J. Res. Med. Sci.* **2018**, *23*, 63.

(9) Yuan, Y.; Lee, R. E.; Besra, G. S.; Belisle, J. T.; Barry, C. E., 3rd Identification of a gene involved in the biosynthesis of cyclopropanated mycolic acids in Mycobacterium tuberculosis. *Proc. Natl. Acad. Sci. U.S.A.* **1995**, *92* (14), 6630−6634.

(10) Daffe, M.; Draper, P. The envelope layers of mycobacteria with reference to their pathogenicity. *Adv. Microb. Physiol.* **1997**, *39*, 131−203.

(11) Schleicher, G. K.; Feldman, C.; Vermaak, Y.; Verschoor, J. A. Prevalence of Anti-mycolic Acid Antibodies in Patients with Pulmonary Tuberculosis Co-infected with HIV. *J. Clin. Chem. Lab. Med.* **2002**, *40*, 882−887.

(12) Thanyani, S. T.; Roberts, V.; Siko, D. G. R.; Vrey, P.; Verschoor, J. A. A novel application of affinity biosensor technology to detect antibodies to mycolic acid in tuberculosis patients. *J. Immunol. Methods* **2008**, *332*, 61−72.

(13) Jacobo-Delgado, Y. M.; Rodríguez-Carlos, A.; Serrano, C. J.; Rivas-Santiago, B. Mycobacterium tuberculosis cell-wall and anti-microbial peptides: a mission impossible? *Front. Immunol.* **2023**, *14*, 1194923.

(14) Bansal-Mutalik, R.; Nikaido, H. Mycobacterial outer membrane is a lipid bilayer and the inner membrane is unusually rich in diacyl phosphatidylinositol dimannosides. *Proc. Natl. Acad. Sci. U.S.A.* **2014**, *111*, 4958−4963.

(15) Minnikin, D. E.; Minnikin, S. M.; Goodfellow, M.; Stanford, J. L. The Mycolic Acids of Mycobacterium chelonei. *Microbiology* **1982**, *128*, 817−822.

(16) Hett, E. C.; Rubin, E. J. Bacterial growth and cell division: a mycobacterial perspective. *Microbiol. Mol. Biol. Rev.* **2008**, *72* (1), 126−156.

(17) Vollmer, W.; Blanot, D.; De Pedro, M. A. Peptidoglycan structure and architecture. *FEMS Microbiol. Rev.* **2008**, *32* (2), 149−167.

(18) Kalscheuer, R.; Palacios, A.; Anso, I.; Cifuente, J.; Anguita, J.; Jacobs, W. R.; Guerin, M. E.; Prados-Rosales, R. The Mycobacterium tuberculosis capsule: a cell structure with key implications in pathogenesis. *Biochem. J.* **2019**, *476* (14), 1995−2016.

(19) Watanabe, M.; Aoyagi, Y.; Ridell, M.; Minnikin, D. E. Separation and characterization of individual mycolic acids in representative mycobacteria. *Microbiology* **2001**, *147*, 1825−1837.

(20) Villeneuve, M.; Kawai, M.; Kanashima, H.; Watanabe, M.; Minnikin, D. E.; Nakahara, H. Temperature dependence of the Langmuir monolayer packing of mycolic acids from Mycobacterium tuberculosis. *Biochim. Biophys. Acta* **2005**, *1715*, 71−80.

(21) Villeneuve, M.; Kawai, M.; Watanabe, M.; Aoyagi, Y.; Hitotsuyanagi, Y.; Takeya, K.; Gouda, H.; Hirono, S.; Minnikin, D. E.; Nakahara, H. Differential conformational behaviors of α-mycolic acids in Langmuir monolayers and computer simulations. *Chem. Phys. Lipids* **2010**, *163*, 569−579.

(22) Villeneuve, M.; Kawai, M.; Horiuchi, K.; Watanabe, M.; Aoyagi, Y.; Hitotsuyanagi, Y.; Takeya, K.; Gouda, H.; Hirono, S.; Minnikin, D. E. Conformational folding of mycobacterial methoxy- and ketomycolic acids facilitated by alpha-methyl trans-cyclopropane groups rather than cis-cyclopropane units. *Microbiology.* **2013**, *159*, 2405−2415.

(23) Mathebula, N. S.; Pillay, J.; Toschi, G.; Verschoor, J. A.; Ozoemena, K. I. Recognition of anti-mycolic acid antibody at self-assembled mycolic acid antigens on a gold electrode: a potential impedimetric immunosensing platform for active tuberculosis. *Chem. Commun.* **2009**, *23*, 3345−3347.

(24) Maphanga, C.; Manoto, S.; Ombinda-Lemboumba, S.; Ismail, Y.; Mthunzi-Kufa, P. Localized surface plasmon resonance biosensing of Mycobacterium tuberculosis biomarker for TB diagnosis. *Sens. Biosens. Res.* **2023**, *39*, 100545.

(25) Viader-Salvadó, J. M.; Molina-Torres, C. A.; Guerrero-Olazarán, M. Detection and identification of mycobacteria by mycolic acid analysis of sputum specimens and young cultures. *J. Microbiol. Methods* **2007**, *70*, 479−483.

(26) Benadie, Y.; Deysel, M.; Siko, G. R.; Roberts, V.; Van Wyngaardt, S.; Thanyani, S. T.; Sekanka, G.; Ten Bokum, A. M. C.; Collett, L. A.; Grooten, J.; Baird, M. S.; Verschoor, J. A.; Verschoor, J. A. Cholesteroid nature of free mycolic acids from M. tuberculosis. *Chem. Phys. Lipids* **2008**, *152*, 95−103.

(27) Ranchod, H.; Ndlandla, F.; Lemmer, Y.; Beukes, M.; Niebuhr, J.; Al-Dulayymi, J.; Wemmer, S.; Fehrsen, J.; Baird, M.; Verschoor, J. The antigenicity and cholesteroid nature of mycolic acids determined by recombinant chicken antibodies. *PLoS One* **2018**, *13* (8), No. e0200298.

(28) Mashaghi, S.; Jadidi, T.; Koenderink, G.; Mashaghi, A. Lipid Nanotechnology. *Int. J. Mol. Sci.* **2013**, *14* (2), 4242−4282.

(29) Akbarzadeh, A.; Rezaei-Sadabady, R.; Davaran, S.; Joo, S. W.; Zarghami, N.; Hanifehpour, Y.; Samiei, M.; Kouhi, M.; Nejati-Koshki,

https://doi.org/10.1021/acsomega.5c00904
ACS Omega 2025, 10, 50813−50824

K. Liposome: classification, preparation, and applications. *Nanoscale Res. Lett.* **2013**, *8* (1), 102.
(30) Wang, J.; El-Sayed, M. A. Time-Resolved Fourier Transform Infrared Spectroscopy of the Polarizable Proton Continua and the Proton Pump Mechanism of Bacteriorhodopsin. *Biophys. J.* **2001**, *80*, 961−971.
(31) Baker, M. J.; Byrne, H. J.; Chalmers, J.; Gardner, P.; Goodacre, R.; Henderson, A.; Kazarian, S. G.; Martin, F. L.; Moger, J.; Stone, N.; Sulé-Suso, J. Clinical applications of infrared and Raman spectroscopy: state of play and future challenges. *Analyst* **2018**, *143*, 1735−1757.
(32) Kiran, S.; Satish-Kumar, M.; Nakamura, Y.; Hokada, T. Comparison between Raman spectra of carbonaceous material and carbon isotope thermometries in low-medium grade meta-carbonates: Implications for estimation of metamorphic temperature condition. *Precambrian Res.* **2022**, *374*, 106656.
(33) Hamada, Y.; Getahun, H.; Tadesse, B. T.; Ford, N. HIV-associated tuberculosis. *Int. J. STD AIDS* **2021**, *32* (9), 780−790.
(34) Ozoemena, K. I.; Mathebula, N. S.; Pillay, J.; Toschi, G.; Verschoor, J. A. Electron transfer dynamics across self-assembled N-(2-mercaptoethyl) octadecanamide/mycolic acid layers: impedimetric insights into the structural integrity and interaction with anti-mycolic acid antibodies. *Phys. Chem. Chem. Phys.* **2010**, *12*, 345−357.
(35) Gelpi, M.; Afzal, S.; Lundgren, J.; Ronit, A.; Roen, A.; Mocroft, A.; Gerstoft, J.; Lebech, A.; Lindegaard, B.; Kofoed, K. F.; Nordestgaard, B. G.; Nielsen, S. D. Higher Risk of Abdominal Obesity, Elevated Low-Density Lipoprotein Cholesterol, and Hypertriglyceridemia, but not of Hypertension, in People Living With Human Immunodeficiency Virus (HIV): Results From the Copenhagen Comorbidity in HIV Infection Study. *Clin. Infect. Dis.* **2018**, *67* (4), 579−586.
(36) Mofokeng, T. P.; Tetana, Z. N.; Ozoemena, K. I. Defective 3D nitrogen-doped carbon nanotube-carbon fibre networks for high performance supercapacitor: Transformative role of nitrogen-doping from surface-confined to diffusive kinetics. *Carbon* **2020**, *169*, 312−326.
(37) Pillay, J.; Ozoemena, K. I. Layer-by-layer self-assembled nanostructured phthalocyaninatoiron(II)/SWCNT-poly(m-aminobenzenesulfonic acid) hybrid system on gold surface: Electron transfer dynamics and amplification of H2O2 response. *Electrochim. Acta* **2009**, *54*, 5053−5059.
(38) Maxakato, N. W.; Arendse, C. J.; Ozoemena, K. I. Insights into the electro-oxidation of ethylene glycol at Pt/Ru nanocatalysts supported on MWCNTs: Adsorption-controlled electrode kinetics. *Electrochem. Commun.* **2009**, *11*, 534−537.
(39) Mofokeng, T. P.; Ipadeola, A. K.; Tetana, Z. N.; Ozoemena, K. I. Defect-Engineered Nanostructured Ni/MOF-Derived Carbons for an Efficient Aqueous Battery-Type Energy Storage Device. *ACS Omega* **2020**, *5*, 20461−20472.
(40) Orazem, M. E.; Tribollet, B. *Electrochemical Impedance Spectroscopy*; Wiley, 2017.
(41) Monk, P. M. *Fundamentals of Electroanalytical Chemistry*; John Wiley & Sons, 2008.
(42) Bard, A. J.; Faulkner, L. R. *Electrochemical Methods: Fundamentals and Applications*; Wiley, 2001.
(43) Compton, R. G.; Banks, C. E. *Understanding Voltammetry*; World Scientific, 2018.
(44) Peteni, S.; Ozoemena, O. C.; Khawula, T.; Haruna, A. B.; Rawson, F. J.; Shai, L. J.; Ola, O.; Ozoemena, K. I. Electrochemical Immunosensor for Ultra-Low Detection of Human Papillomavirus Biomarker for Cervical Cancer. *ACS Sens.* **2023**, *8*, 2761−2770.
(45) Maalouf, R.; Fournier-Wirth, C.; Coste, J.; Chebib, H.; Saïkali, Y.; Vittori, O.; Errachid, A.; Cloarec, J. P.; Martelet, C.; Jaffrezic-Renault, N. Label-Free Detection of Bacteria by Electrochemical Impedance Spectroscopy: Comparison to Surface Plasmon Resonance. *Anal. Chem.* **2007**, *79*, 4879−4886.

https://doi.org/10.1021/acsomega.5c00904
ACS Omega 2025, 10, 50813−50824